Electronic Supplementary Material (ESI) for Energy Advances.
This journal is © The Royal Society of Chemistry 2022

Supplementary Information

Single crystal Ni-rich NMC cathode materials for lithium-ion batteries with ultra-high volumetric energy density

Ivan A. Moiseev[a], Aleksandra A. Savina[a], Alina D. Pavlova[a], Tatiana A. Abakumova[b],
Vladislav S. Gorshkov[a], Egor M. Pazhetnov[a], Artem M. Abakumov[a]*
a – Center for Energy Science and Technology, Skolkovo Institute of Science and Technology, Nobel Str. 3, 121205 Moscow, Russia
b – Rustor Ltd, Skolkovo Innovation Center, Bolshoi blv 43-1, 121205 Moscow, Russia

Synthesis

The mixed transition metal hydroxide precursors $Ni_xMn_yCo_{1-x-y}(OH)_2$ (x = 0.6, 0.8, y = 0.2, 0.1) were synthesized via a conventional co-precipitation method. Aqueous solutions of TM sulfates ($NiSO_4 \cdot 7H_2O$, $MnSO_4 \cdot H_2O$, $CoSO_4 \cdot 5H_2O$, Alfa Aesar, 99%) taken in a stoichiometric ratio with the total concentration of 2 mol/L were slowly pumped into a 5L continuously stirred batch reactor under Ar atmosphere. Simultaneously, aqueous solution of 4 mol/L NaOH (Alfa Aesar, 99%) and $NH_3 \cdot H_2O$ (Alfa Aesar) were separately pumped into the reactor as the precipitating and complexing agents, respectively. The temperature of the reactor was maintained at 50°C while pH was fixed at 11.0 for the x = 0.6 precursor and 11.5 for the x = 0.8 precursor. After co-precipitation, the resulting reaction mixture was kept at 50°C under stirring at 1000 rpm for about 24 h for aging.

In order to obtain the single crystal SC622 and SC811 samples, the prepared precursors, $LiOH \cdot H_2O$ (Alfa Aesar, 99%) and K_2SO_4 (Alfa Aesar, 99.9%) with molar ratio of 0.2:0.3:0.075 were mixed, annealed at 900°C for 10 h and then cooled at a rate of 2°C/min to 300°C. After that, the mixture was allowed to cool down together with the furnace. The obtained powders were ground, washed using deionized water to separate the material from the water-soluble K-/ Li-salts, centrifuged and dried at 80°C for ~12 h. The final SC622 and SC811 powders were obtained by annealing at 700 °C for 6 h. Another portion of the mixed precursors was used to synthesize the polycrystalline samples PC622 and PC811. The hydroxide precursors were mixed with $LiOH \cdot H_2O$ in a molar ratio of 1:1.05 and annealed at either 500 °C for 5 h and then at 850 °C for 12 h with intermediate grinding between the calcination steps to prepare PC622 or at 750°C for 12 h to produce PC811. In both single crystal and polycrystalline cases, the SC/PC622 samples were obtained in air, while the SC/PC811 materials were synthesized in flowing oxygen.

Characterization

Powder X-ray diffraction (PXRD) patterns were recorded with a Bruker D8 Advanced diffractometer (CuK_α, λ_1 = 1.54056 Å, λ_2 = 1.54439 Å) equipped with an energy-dispersive LYNXEYE XE position-sensitive detector. The unit cell parameters and the degree of Ni^{2+}/Li^+ disorder, originated from a partial exchange of the Li^+ (r_{IV} = 0.76 Å) and Ni^{2+}(r_{IV} = 0.69 Å) cations between the 3*b* (i.e., Li) and 3*a* (i.e.,Ni) sites were calculated using Rietveld refinement from powder XRD data [1] with the JANA2006 program package [2].

Particle morphology, size distribution and cross-sections of the electrodes were investigated by scanning electron microscopy (SEM) using a ThermoFisher Quattro S microscope.

Tap density was determined with a tapped density analyzer Quantachrome Autotap. At least 20 g of powder was poured into a 25 ml glass cylinder and the cylinder was tapped 3000 times before measuring the sample volume.

The powder compact density was measured by pressing 1 g of powders into pellets using custom mold with 13 mm diameter under a pressure of 5 t/cm^2. After pressing the thickness of pellets was measured by an electronic micrometer to calculate their volume (V).

Samples for transmission electron microscopy (TEM) studies were prepared in air by crushing the crystals with an agate mortar and pestle under ethanol and depositing a drop of suspension onto a carbon film supported by a copper grid. High angle annular dark field scanning transmission electron microscopy (HAADF-STEM) images as well as EDX maps were acquired on a ThermoFisher Titan Themis Z electron microscope at 200 kV equipped with a Super-X system for EDX analysis.

X-ray photoelectron spectroscopy (XPS) experiments were performed using a PHI 500 VersaProbe II spectrometer with spherical mirror analyzers. A monochromatic Al K_α X-ray source was used. Pressure in the analysis chamber was in the range of 10^{-6} –10^{-7} Pa. High resolution XPS spectra were recorded with 0.1eV step size, processed, calibrated and normalized to the same spectra height for comparison. C1s at 285.0 eV binding energy position of adventitious carbon on the surface of sample particles was used as the reference for energy calibration of all the spectra.

The electrochemical properties were tested in coin-type 2032 cells using a BTS4000-5V10mA Battery Testing System (Neware) with lithium metal as a counter electrode. The active cathode material, conductive additive (Super-P), and binder (polyvinylidene-fluoride, PVDF, Solvay Solef 5130) were suspended in N-methyl-2-pyrrolidone (NMP) with a weight ratio of 80:10:10 and homogenized to form a slurry. The obtained slurry was applied onto a carbon-coated Al current collector (TOB) using an automatic film applicator Zehntner ZAA 2300, dried at 110°C until complete evaporation of NMP for 12 hours, calendared and then punched into 15 mm diameter disks with the cathode loading of ~3 mg/cm^2. The electrolyte consisting of 1M $LiPF_6$ (Sigma-Aldrich, 99.99%) solution in ethylene carbonate/propylene carbonate/dimethyl carbonate solution (EC:PC:DMC = 1:1:3 vol.) was used. The half-cells were assembled in an Ar-filled glove box, and galvanostatic tests were performed in the potential range of 2.7–4.3 V vs. Li/Li^+ at room temperature at different current densities.

Electrochemical impedance spectroscopy (EIS) measurements were performed in a three-electrode cell configuration with lithium metal as a counter and reference electrode. Tests were conducted using a Biologic VMP3 potentiostat in the frequency range from 100 kHz to 10 mHz with the amplitude of AC signal of 5 mV at 3.8 V. For approximation of obtained EIS spectra the typical equivalent circuit for Li-ion battery was used, which includes contributions from the electrolyte solution resistance (R_{sol}), interface resistance and capacitance (R_{SEI} and C_{SEI}), charge transfer resistance (R_{ct}), double layer capacitance (C_{dl}) and Warburg element (W) for diffusion. For better fitting, constant phase elements (CPE) were used instead of classical capacitors for C_{SEI} and C_{dl}.

The electrodes for microstructure investigation were prepared similarly to the cathodes for half-cells. The active cathode material, conductive additive (Super-P), binder (polyvinylidene-fluoride, PVDF, Solvay Solef 5130), and carbon nanotubes (TUBALL^{TM}) were suspended in N-methyl-2-pyrrolidone (NMP) with a weight ratio of 89:4.9:6:0.1 and homogenized to form a slurry. The obtained slurry was applied onto a carbon-coated Al current collector (TOB) using an automatic film applicator Zehntner ZAA 2300, dried at 110°C until complete evaporation of NMP for 12 hours, calendared and then punched into 12 mm diameter disks with the cathode loading of ~14.65 mg/cm^2, ~14.90 mg/cm^2, ~14.66 mg/cm^2, ~14.30 mg/cm^2 for PC622, SC622, PC811 and SC811 respectively. The electrode compact density was measured by cathodes pressing using custom mold with 13 mm diameter under pressure of 2, 4 and 8 t/cm^2.

Full cells were assembled with the SC622 and SC811 cathodes and $Li_4Ti_5O_{12}$ (LTO) anode. Cathodes for full cells were prepared similarly to the cathodes for half-cells, mass loading was 2.8-3.2 mg/cm^2. The active anode material (commercially available LTO (TOB)), conductive additive (Super-P), and PVDF binder were suspended in NMP with a weight ratio of 92:3:5 and homogenized to form a slurry. The obtained slurry was applied onto a carbon-coated Al current collector, dried, and then cut into 15 mm diameter disks with the anode loading of 3.1-3.5 mg/cm^2. The electrolyte consisting of 1 M $LiPF_6$ solution in ethylene carbonate/ethyl methyl carbonate solution (EC:EMC = 2:5 by weight) + 2 w.% of vinylene carbonate was used. 3-layer polyethylene/polypropylene/polyethylene Celgard 2325 film with a thickness of 25 μm was used as a separator. The full-cells were assembled in an Ar-filled glove box and rested for 12h at room temperature to ensure good wetting. Full-cell formation was performed by carrying out three charge-discharge cycles in galvanostatic mode at 0.1C, 0.3C and 0.5C in the potential range of 1.60–2.65 V in thermostatic test chamber MHWX-200 (Neware) at 25 °C. Capacity retention tests were performed right after formation in the same potential range at 1C in CC-CV charge (1C constant current till 2.65 V and constant voltage at 2.65V till 0.05C) and CC discharge (1C constant current till 1.60 V) mode at 25 °C.

Description of the Co2p$_{3/2}$ and Mn3p XPS spectra.

Transition metal ions show multiplet splitting together with prominent losses in a process of photoelectron emission. This is why their photoelectron spectra shapes are very complex and asymmetric (Figure S8). The XPS spectra from the SC622/811 and PC622/811 samples evidence that the oxidation state of cobalt at the surface is +3. This is supported by the main peak positioned at 780.2eV and an additional small loss peak at 790.1 eV. These peak positions are close to the ones in $LiCoO_2$ [3]. Analysis of Mn2p$_{3/2}$ photoelectron line in NMCs is essentially hampered by its overlap with the strong and broad Auger line from the Ni ions. Thus, the Mn3p photoelectron line has been chosen for analysis. XPS gives central positions of the Mn3p photoelectron line at 50.0eV for all the samples. This position can be attributed to Mn^{4+} in oxides [4].

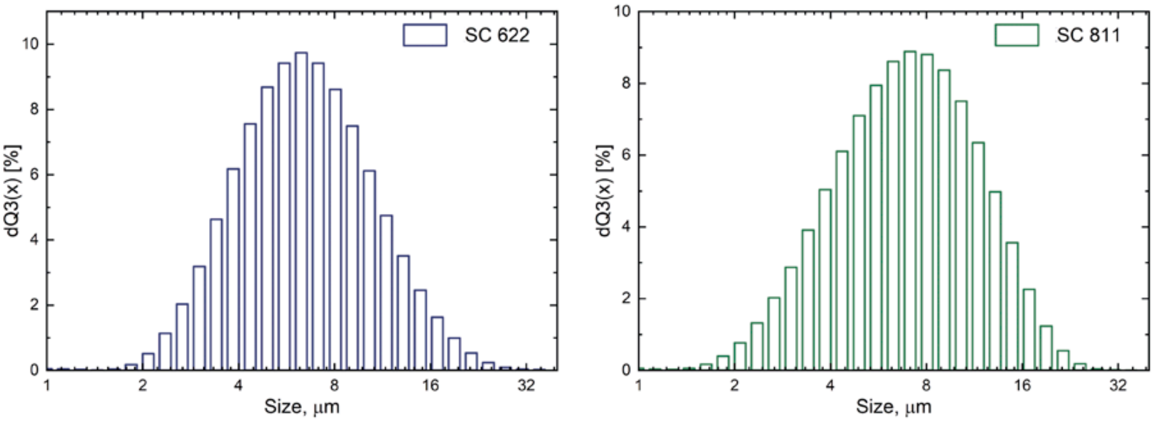

Figure S1. Particle size distribution for the SC622 (D10/D50/D90 = 3.4/6.4/12.2 µm) (left) and SC811 (D10/D50/D90 = 3.2/7.0/13.2 µm) (right) samples.

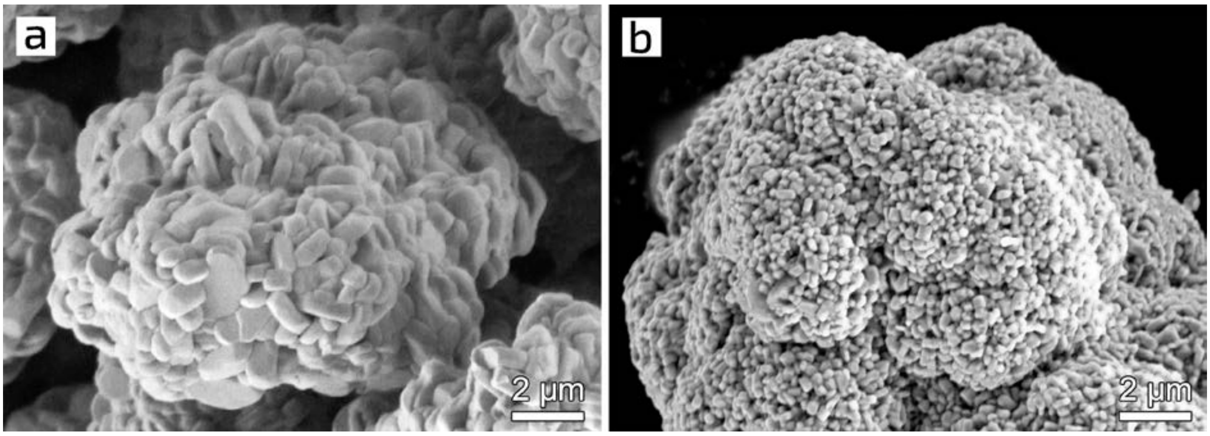

Figure S2. SEM images of the PC622 (a) and PC811 (b) samples.

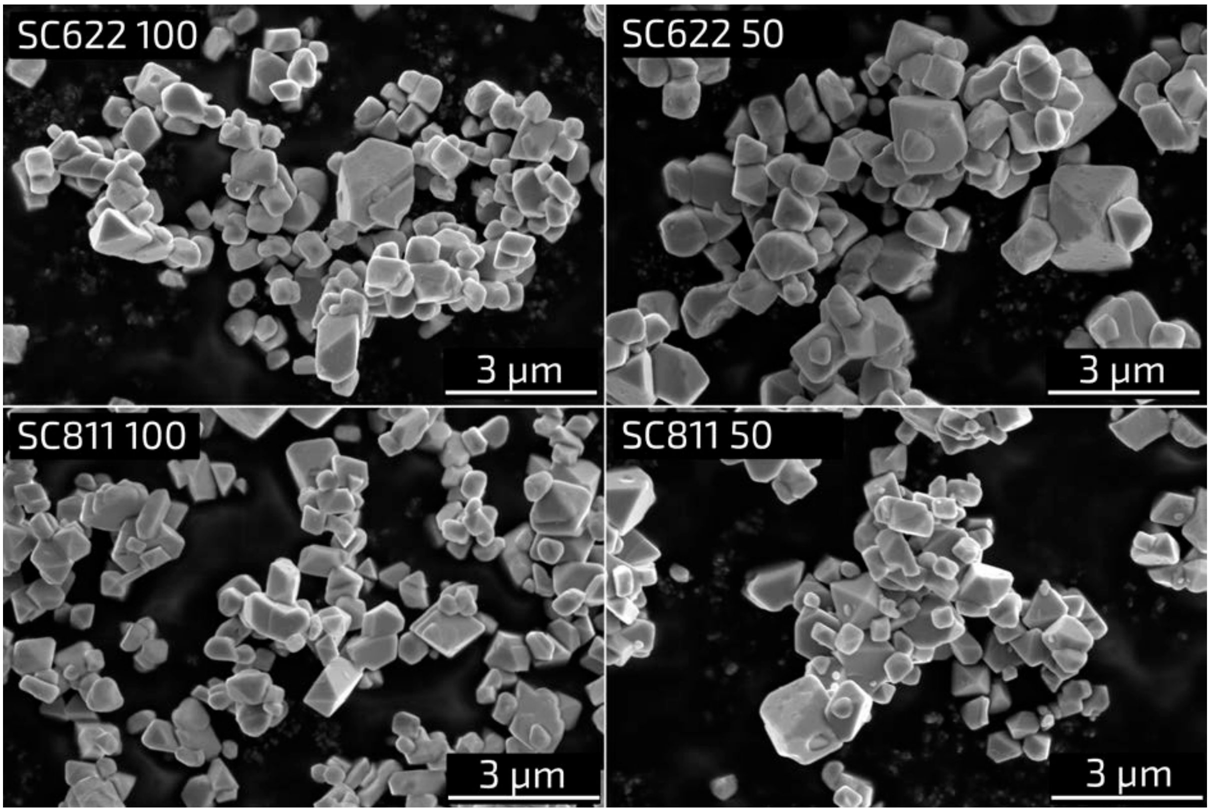

Figure S3. SEM images of the SC622_100, SC622_50, SC811_100 and SC811_50 samples.

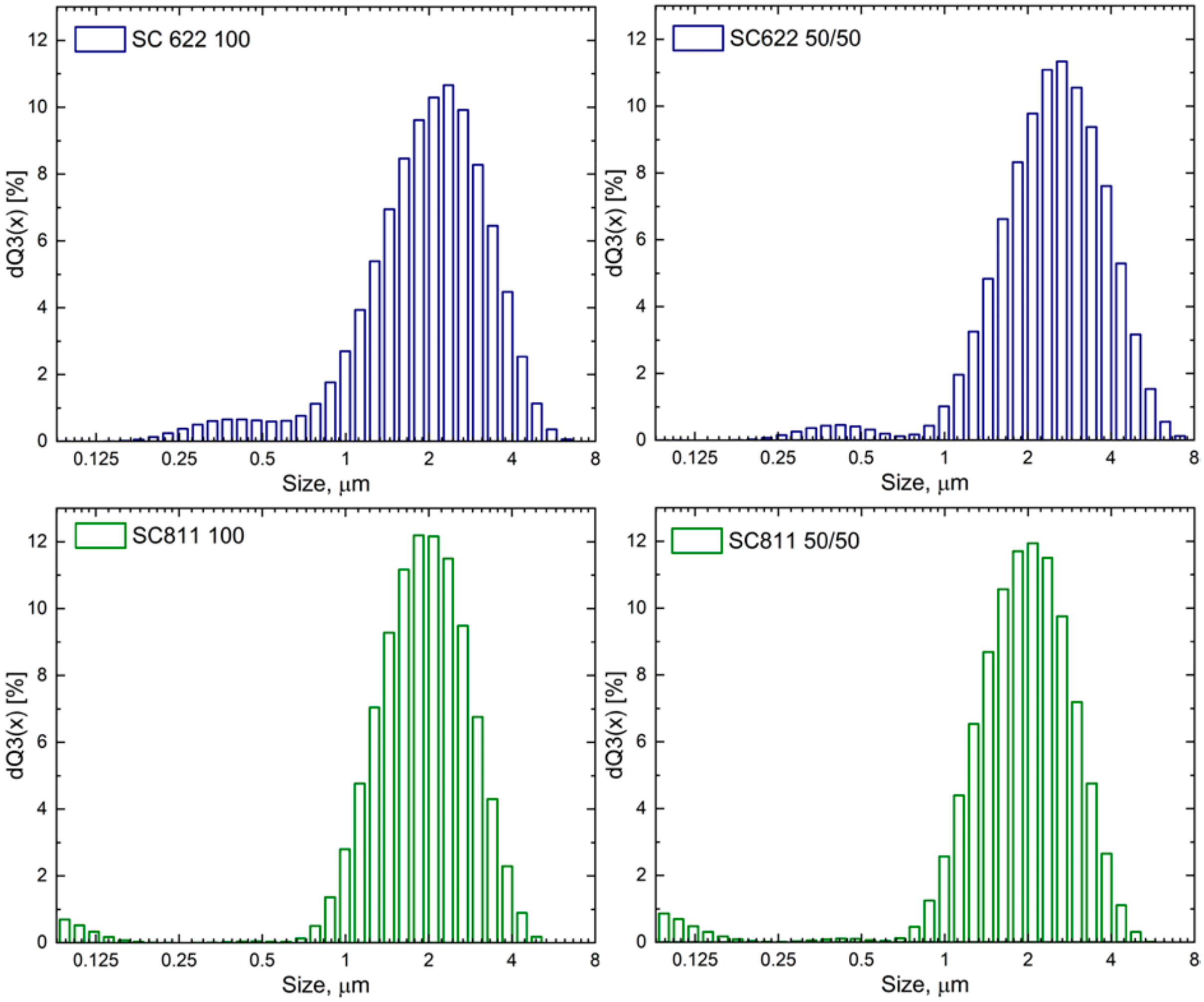

Figure S4. Particle size distributions for the SC622_100, SC622_50, SC811_100 and SC811_50 samples.

Table S1. D10/D50/D90 and tap densities for the SC622_100, SC622_50, SC811_100 and SC811_ 50 samples. The data for the SC622 and SC811 samples prepared without Li_2CO_3 are given for comparison.

Sample	D10, μm	D50, μm	D90, μm	Tap density, g/cm^3
SC622_100	1.0	2.3	4.1	1.8
SC622_50	1.4	2.8	4.7	1.65
SC811_100	1.2	2.0	3.3	1.3
SC811_50	1.2	2.1	3.5	1.4
SC622	3.4	6.4	13.2	3.0
SC811	3.2	7.0	13.2	2.9

Table S2. Crystallographic data after the Rietveld refinement for the single crystal SC622, SC811 and polycrystalline PC622 and PC811 samples.

Parameter	SC622	PC622	SC811	PC811
a, Å	2.867327(5)	2.867207(1)	2.873200(7)	2.87333(2)
c, Å	14.21106(5)	14.21561(1)	14.19868(7)	14.2081(2)
V, Å^3	101.1838(2)	101.2079(1)	101.5138(6)	101.587(1)
Ni in 3a site, %	0.8(6)	1.9(4)	1.2(4)	2.4(5)
Li in 3b site, %	1.8(5)	2.1(6)	0.8(5)	2.6(4)
R_F, R_p, R_{wp}	0.025, 0.014, 0.019	0.026, 0.021, 0.026	0.024,0.018, 0.028	0.017, 0.020, 0.026

Table S3. Cationic composition of the obtained samples calculated from EDX data.

Sample	Ni, at. %	Mn, at. %	Co, at. %
SC622	59.6(7)	19.7(5)	20.7(8)
PC622	60.1(4)	19.9(5)	20.0(6)
SC811	79.7(5)	9.9(4)	10.4(6)
PC811	79.2(4)	10.3(3)	9.9(2)

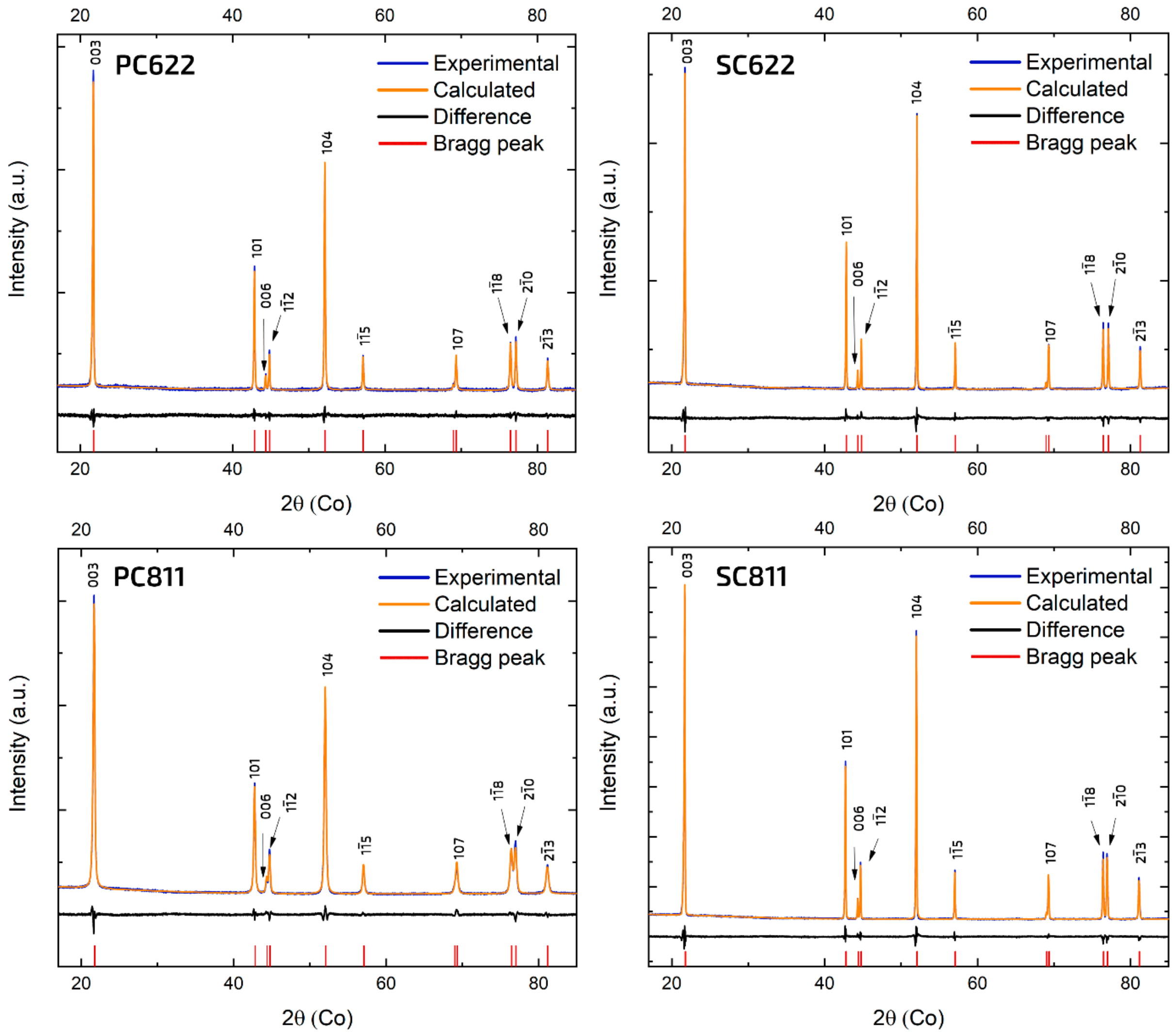

Figure S5. Experimental, calculated, and difference PXRD patterns for the SC and PC samples. Bragg reflection positions for the α-$NaFeO_2$-type structure (sp. gr. *R*-3*m*) are designated with red vertical stripes.

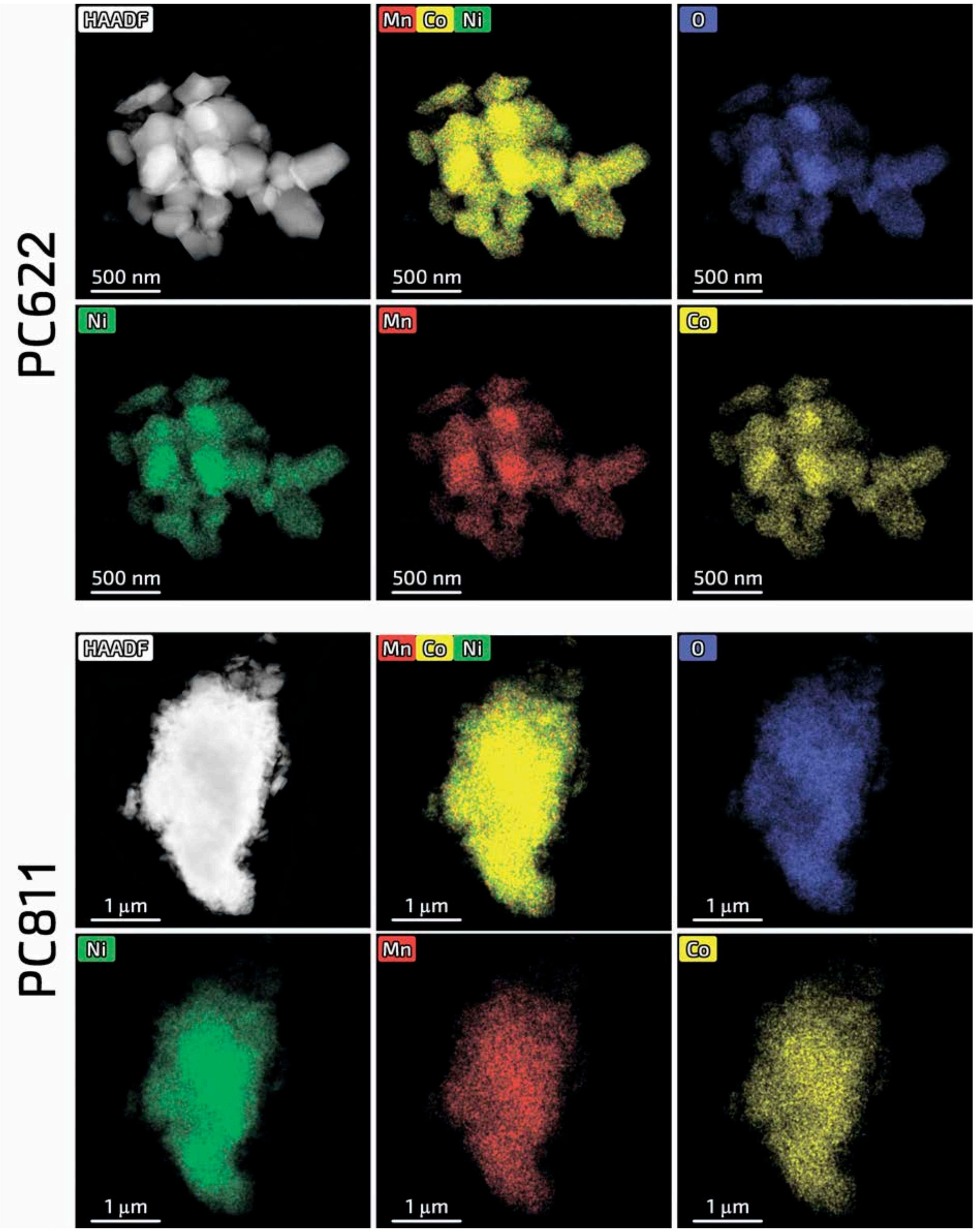

Figure S6. HAADF-STEM images along with the corresponding color-coded elemental maps and the mixed EDX map for Ni, Mn and Co for the polycrystalline samples.

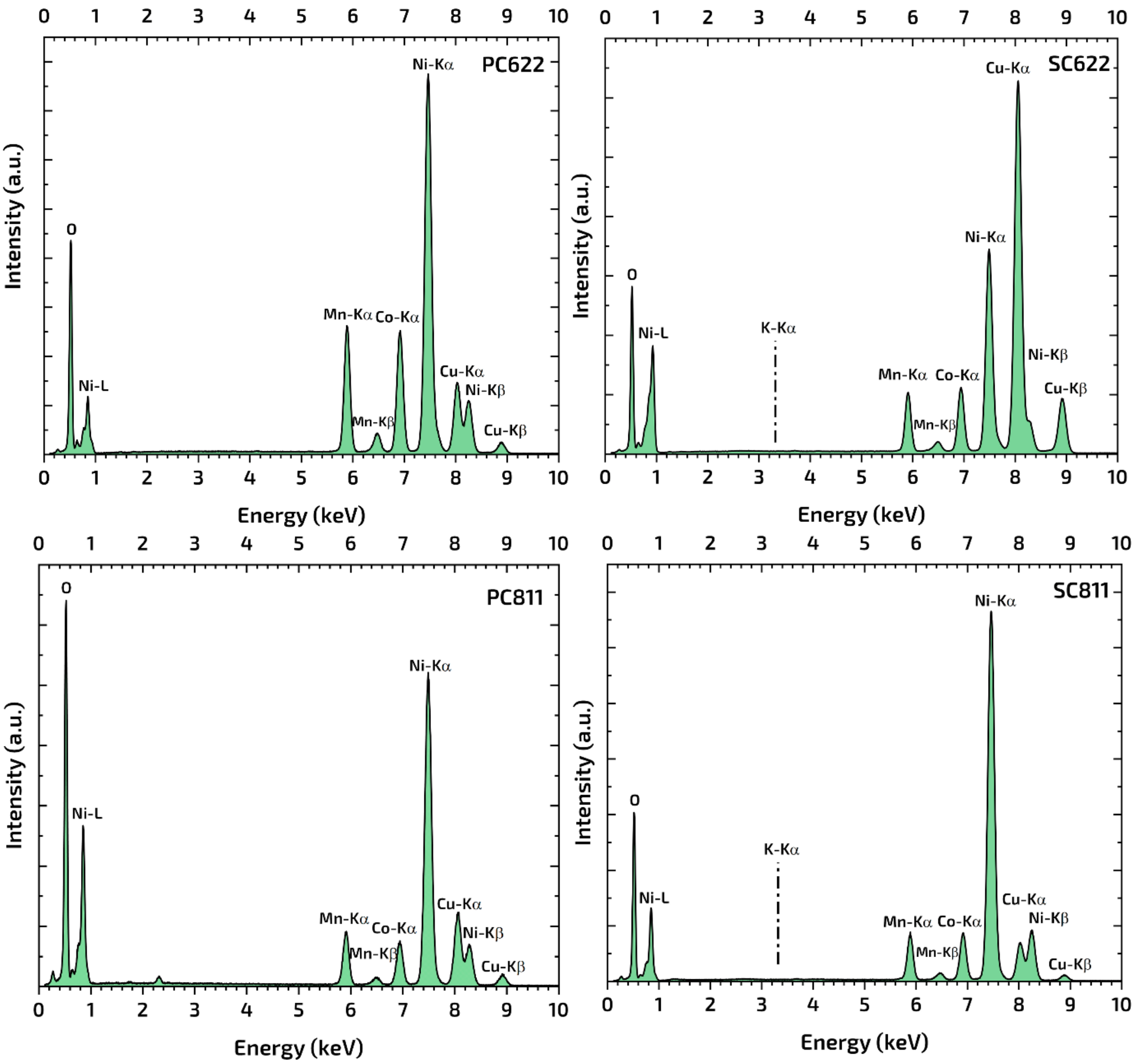

Figure S7. Representative EDX spectra for the obtained samples. The potassium K$_{\alpha1}$ line energy position is marked.

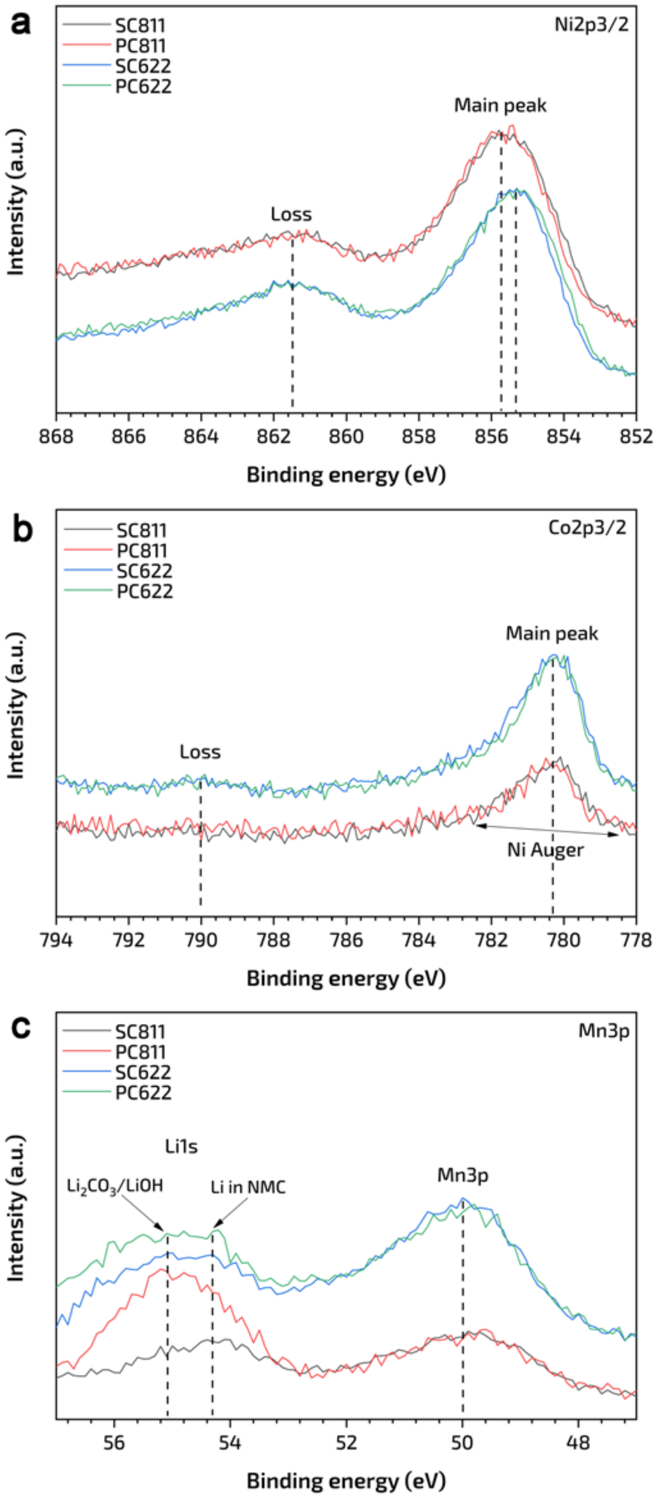

Figure S8. Ni2p$_{3/2}$ (a), Co2p$_{3/2}$ (b) and Mn3p (c) XPS spectra for the SC622/811 and PC622/811 samples.

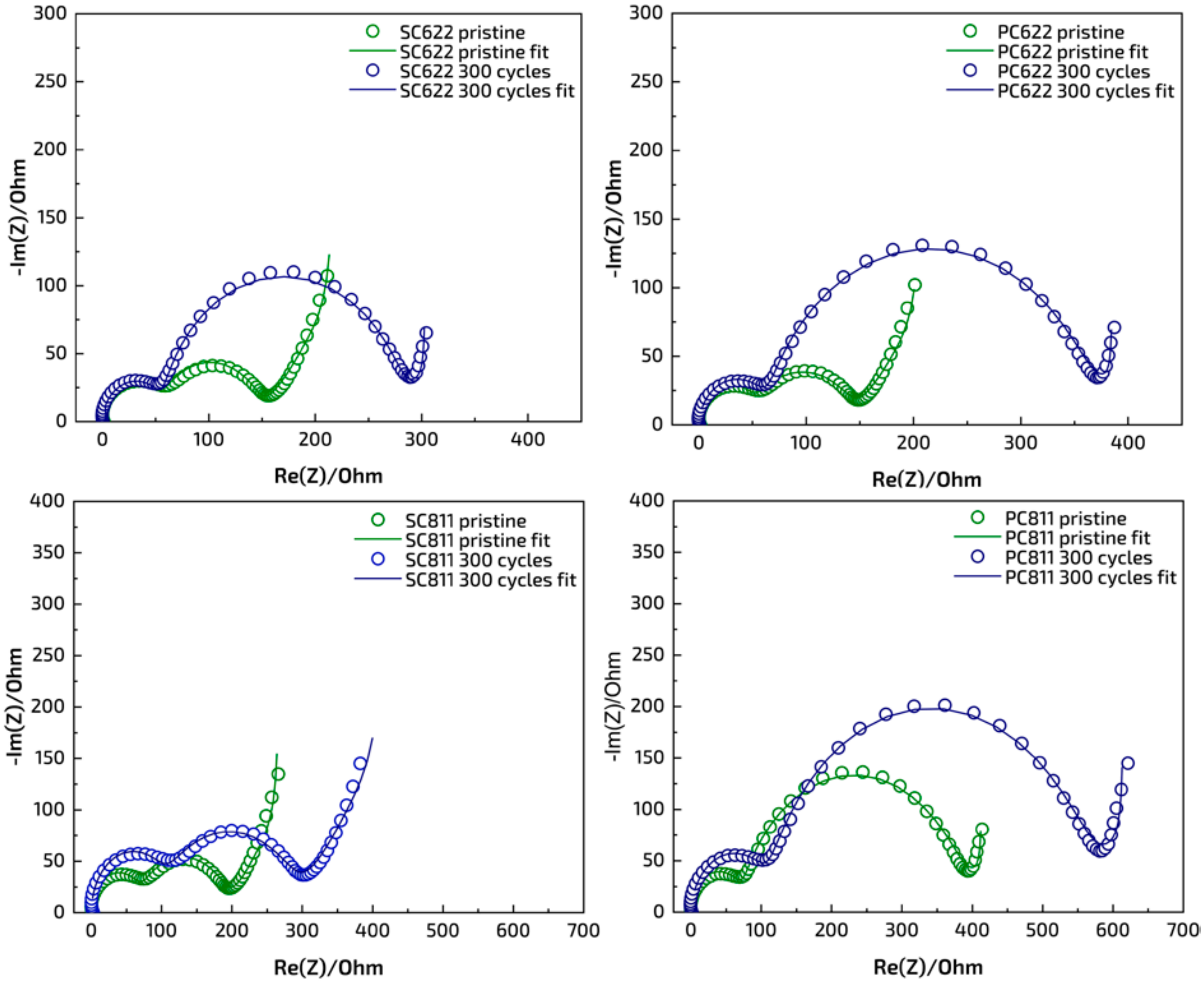

Figure S9. EIS spectra for the pristine electrodes and the electrodes after 300 charge/discharge cycles for the SC622/811 and PC622/811 samples.

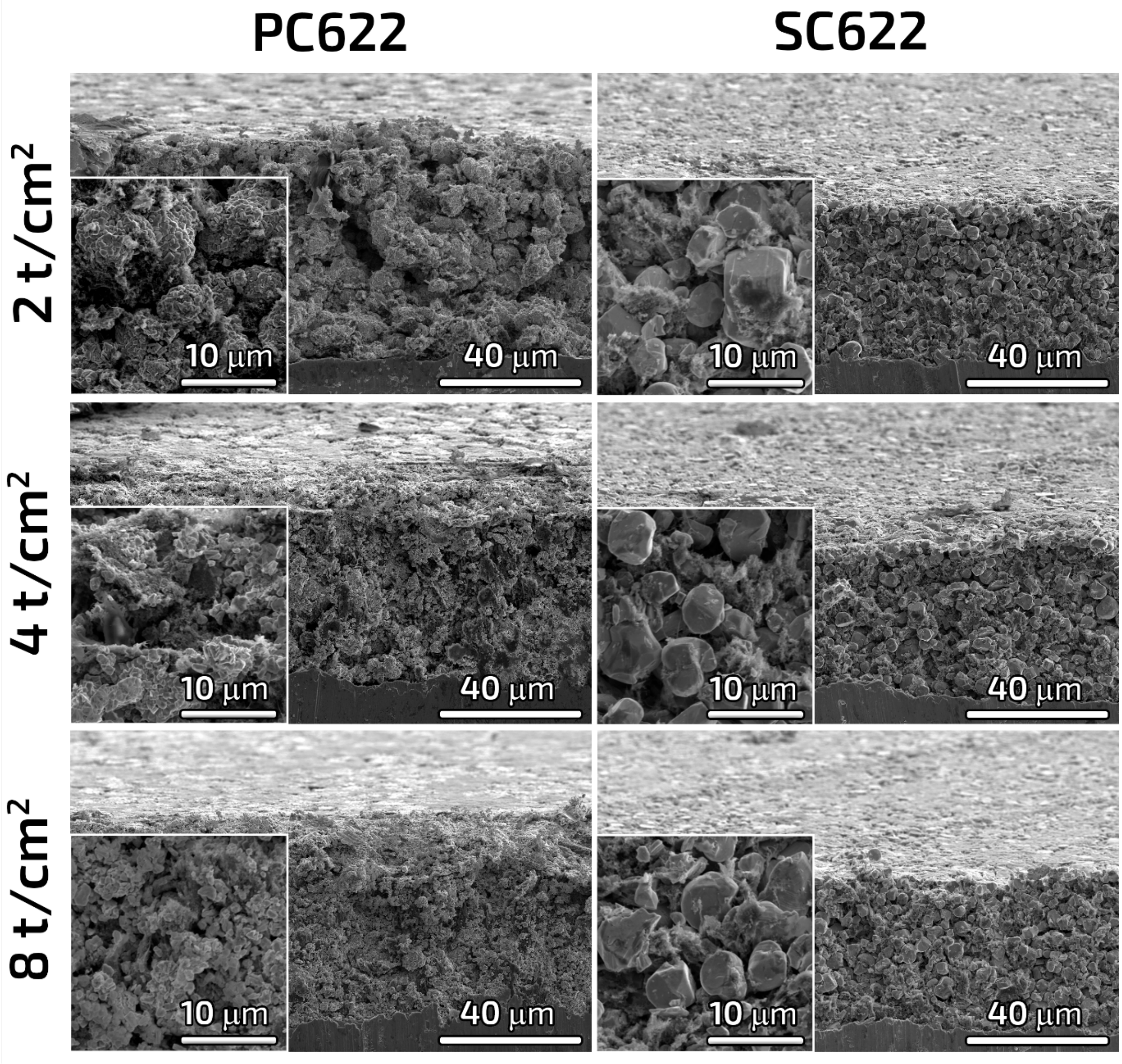

Figure S10. High and low magnification SEM cross-section images of electrodes prepared under 2, 4 and 8 t/cm^2 pressure for PC622 and SC622 samples.

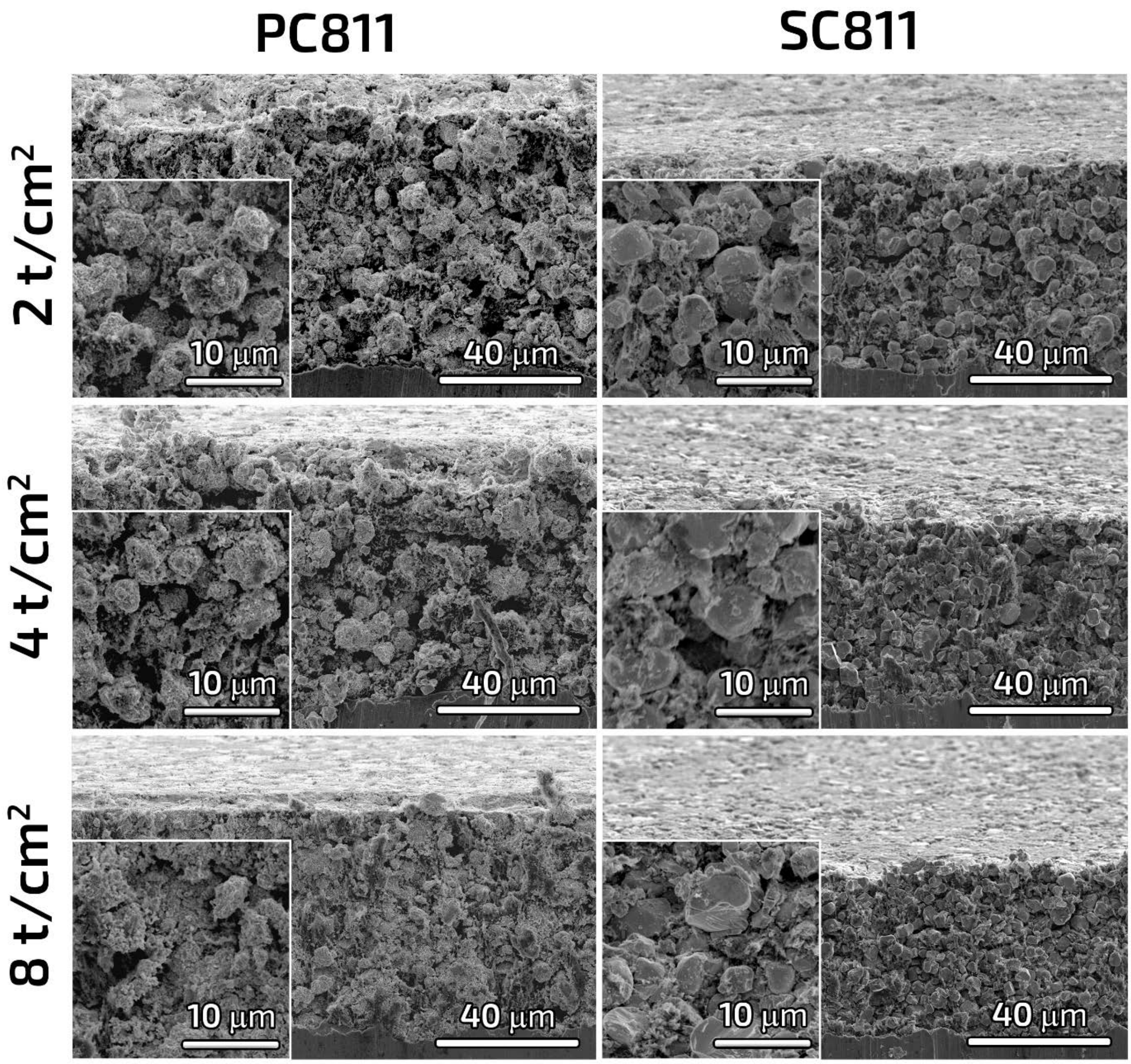

Figure S11. High and low magnification SEM cross-section images of electrodes prepared under 2, 4 and 8 t/cm^2 pressure for PC811 and SC811 samples.

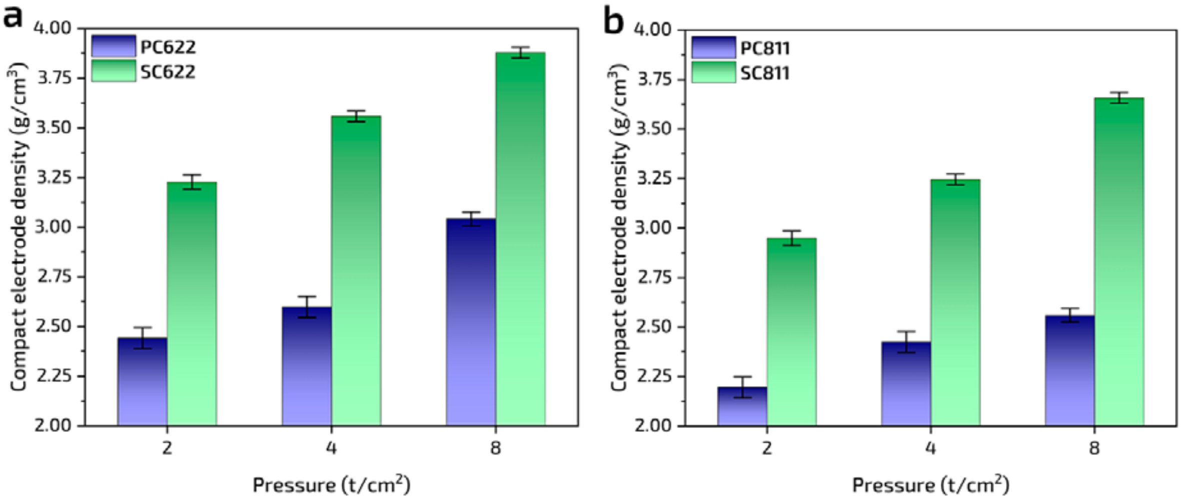

Figure S12. The electrode compact density measured by cathodes pressing under 2, 4, 8 t/cm^2 pressure for (a) – PC622, SC622, (b) – PC811 and SC811 samples.

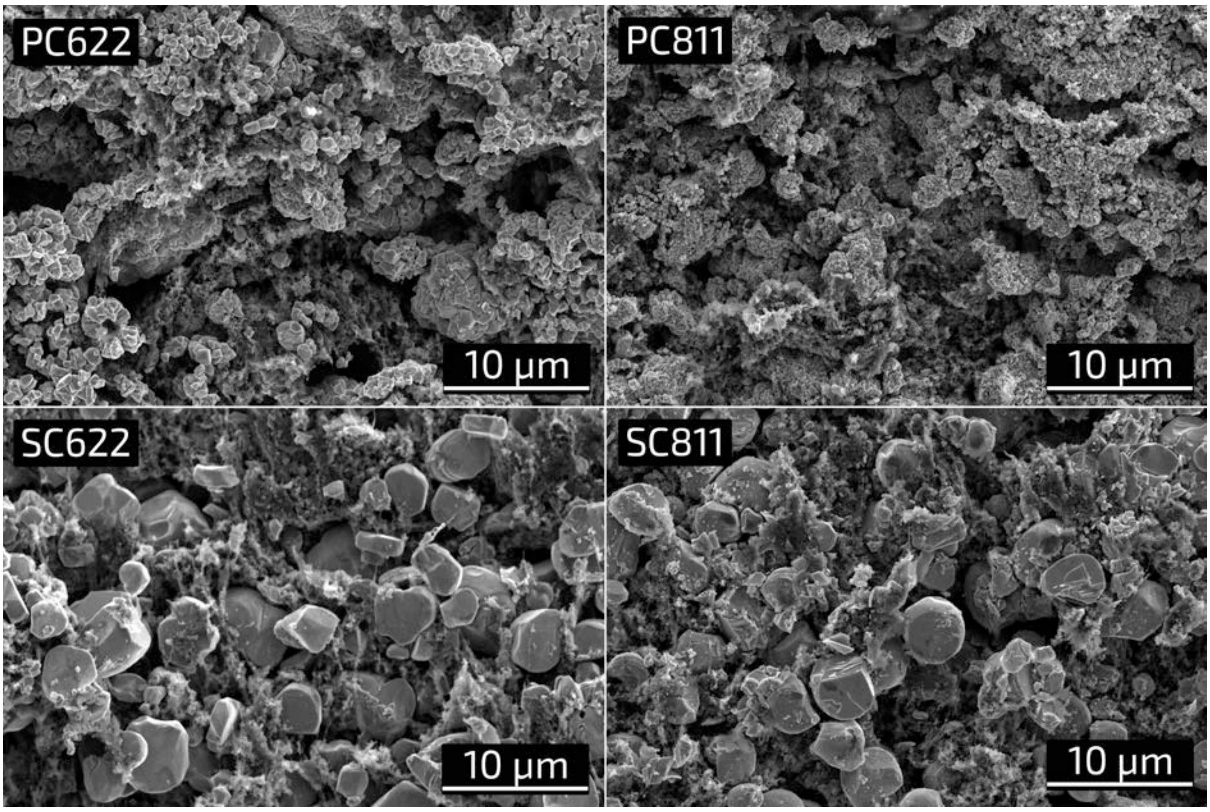

Figure S13. SEM images of the PC622, PC811, SC622 and SC811 electrodes after 300 charge/discharge cycles.

References:

1. E. Orlova, A. Savina, S. Abakumov, A. Morozov, A. Abakumov, *Symmetry*, 2021, **13**, 1628.

2. V. Petříček, M. Dušek, & L. Palatinus, *Zeitschrift für Krist. - Cryst. Mater*., 2014, **229**, 345.
3. Q. Ronald A.; L. Yi-Chun, K. David, S. Yang, M. Azzam N., *J. Electrochem. Soc.*, 2016, **163**, A300.
4. G.C. Allen, S.J. Harris, J.A. Jutson, J.M. Dyke, *Science*, 1989, **37**, 111.